

000 054
 001 055
 002 056
 003 057
 004 058
 005 059
 006 060
 007 061
 008 062
 009 063
 010 064
 011 065
 012 066
 013 067
 014 068
 015 069
 016 070
 017 071
 018 072
 019 073
 020 074
 021 075
 022 076
 023 077
 024 078
 025 079
 026 080
 027 081
 028 082
 029 083
 030 084
 031 085
 032 086
 033 087
 034 088
 035 089
 036 090
 037 091
 038 092
 039 093
 040 094
 041 095
 042 096
 043 097
 044 098
 045 099
 046 100
 047 101
 048 102
 049 103
 050 104
 051 105
 052 106
 053 107

Supplementary File to “Multi-channel Weighted Nuclear Norm Minimization for Real Color Image Denoising”

Anonymous ICCV submission

Paper ID 572

In this supplementary file, we provide:

1. The proof of the Theorem 1 in the main paper.
2. More denoising results on the 24 high quality images from the Kodak PhotoCD dataset.
3. More visual comparisons of denoised images by different methods on the real noisy images of the dataset [1].
4. More visual comparisons of denoised images by different methods on the real noisy images of the dataset [2].

1. Proof of Theorem 1.

Theorem 1. Assume that the weights in w are in a non-descending order, the sequence $\{\mathbf{X}_k\}$, $\{\mathbf{Z}_k\}$, and $\{\mathbf{A}_k\}$ generated in Algorithm 1 satisfy:

$$(a) \lim_{k \rightarrow \infty} \|\mathbf{X}_{k+1} - \mathbf{Z}_{k+1}\|_F = 0; \quad (b) \lim_{k \rightarrow \infty} \|\mathbf{X}_{k+1} - \mathbf{X}_k\|_F = 0; \quad (c) \lim_{k \rightarrow \infty} \|\mathbf{Z}_{k+1} - \mathbf{Z}_k\|_F = 0. \quad (1)$$

Proof. 1. Firstly, we prove that the sequence $\{\mathbf{A}_k\}$ generated by Algorithm 1 is upper bounded. Let $\mathbf{X}_{k+1} + \rho_k^{-1} \mathbf{A}_k = \mathbf{U}_k \Sigma_k \mathbf{V}_k^\top$ be its singular value decomposition (SVD) [3] in the $(k+1)$ -th iteration. According to Corollary 1 of [4], we can have the SVD of \mathbf{Z}_{k+1} as $\mathbf{Z}_{k+1} = \mathbf{U}_k \hat{\Sigma}_k \mathbf{V}_k^\top = \mathbf{U}_k \mathcal{S}_{\frac{w}{\rho_k}}(\Sigma_k) \mathbf{V}_k^\top$. Then we have

$$\|\mathbf{A}_{k+1}\|_F = \|\mathbf{A}_k + \rho_k (\mathbf{X}_{k+1} - \mathbf{Z}_{k+1})\|_F = \rho_k \|\rho_k^{-1} \mathbf{A}_k + \mathbf{X}_{k+1} - \mathbf{Z}_{k+1}\|_F \quad (2)$$

$$= \rho_k \|\mathbf{U}_k \Sigma_k \mathbf{V}_k^\top - \mathbf{U}_k \mathcal{S}_{\frac{w}{\rho_k}}(\Sigma_k) \mathbf{V}_k^\top\|_F = \rho_k \|\Sigma_k - \mathcal{S}_{\frac{w}{\rho_k}}(\Sigma_k)\|_F \quad (3)$$

$$= \rho_k \sqrt{\sum_i (\Sigma_k^{ii} - \mathcal{S}_{\frac{w}{\rho_k}}(\Sigma_k^{ii}))^2} \leq \rho_k \sqrt{\sum_i \left(\frac{w_i}{\rho_k}\right)^2} = \sqrt{\sum_i w_i^2}. \quad (4)$$

The inequality in the second last step can be proved as follows: given the diagonal matrix Σ_k , we define Σ_k^{ii} as the i -th element of Σ_k^{ii} . If $\Sigma_k^{ii} \geq \frac{w_i}{\rho_k}$, we have $\mathcal{S}_{\frac{w}{\rho_k}}(\Sigma_k^{ii}) = \Sigma_k^{ii} - \frac{w_i}{\rho_k} \geq 0$. If $\Sigma_k^{ii} < \frac{w_i}{\rho_k}$, we have $\mathcal{S}_{\frac{w}{\rho_k}}(\Sigma_k^{ii}) = 0 < \Sigma_k^{ii} + \frac{w_i}{\rho_k}$. After all, we have $|\Sigma_k^{ii} - \mathcal{S}_{\frac{w}{\rho_k}}(\Sigma_k^{ii})| \leq \frac{w_i}{\rho_k}$ and hence the inequality holds true. Hence, the sequence $\{\mathbf{A}_k\}$ is upper bounded.

2. Secondly, we prove that the sequence of Lagrangian function $\{\mathcal{L}(\mathbf{X}_{k+1}, \mathbf{Z}_{k+1}, \mathbf{A}_k, \rho_k)\}$ is also upper bounded. Since the global optimal solution of \mathbf{X} and \mathbf{Z} in corresponding subproblems, we always have $\mathcal{L}(\mathbf{X}_{k+1}, \mathbf{Z}_{k+1}, \mathbf{A}_k, \rho_k) \leq \mathcal{L}(\mathbf{X}_k, \mathbf{Z}_k, \mathbf{A}_k, \rho_k)$. Based on the updating rule that $\mathbf{A}_{k+1} = \mathbf{A}_k + \rho_k (\mathbf{X}_{k+1} - \mathbf{Z}_{k+1})$, we have $\mathcal{L}(\mathbf{X}_{k+1}, \mathbf{Z}_{k+1}, \mathbf{A}_{k+1}, \rho_{k+1}) = \mathcal{L}(\mathbf{X}_{k+1}, \mathbf{Z}_{k+1}, \mathbf{A}_k, \rho_k) + \langle \mathbf{A}_{k+1} - \mathbf{A}_k, \mathbf{X}_{k+1} - \mathbf{Z}_{k+1} \rangle + \frac{\rho_{k+1} - \rho_k}{2} \|\mathbf{X}_{k+1} - \mathbf{Z}_{k+1}\|_F^2 = \mathcal{L}(\mathbf{X}_{k+1}, \mathbf{Z}_{k+1}, \mathbf{A}_k, \rho_k) + \frac{\rho_{k+1} + \rho_k}{2\rho_k^2} \|\mathbf{A}_{k+1} - \mathbf{A}_k\|_F^2$. Since the sequence $\{\|\mathbf{A}_k\|_F\}$ is upper bounded, the sequence $\{\|\mathbf{A}_{k+1} - \mathbf{A}_k\|_F\}$ is also upper bounded. Denote by a the upper bound of $\{\|\mathbf{A}_{k+1} - \mathbf{A}_k\|_F\}$, we have $\mathcal{L}(\mathbf{X}_{k+1}, \mathbf{Z}_{k+1}, \mathbf{A}_{k+1}, \rho_{k+1}) \leq \mathcal{L}(\mathbf{X}_1, \mathbf{Z}_1, \mathbf{A}_0, \rho_0) + a \sum_{k=0}^{\infty} \frac{\rho_{k+1} + \rho_k}{2\rho_k^2} = \mathcal{L}(\mathbf{X}_1, \mathbf{Z}_1, \mathbf{A}_0, \rho_0) + a \sum_{k=0}^{\infty} \frac{\mu+1}{2\mu^k \rho_0} \leq \mathcal{L}(\mathbf{X}_1, \mathbf{Z}_1, \mathbf{A}_0, \rho_0) + \frac{a}{\rho_0} \sum_{k=0}^{\infty} \frac{1}{\mu^{k-1}}$. The last inequality holds since $\mu+1 < 2\mu$. Since $\sum_{k=0}^{\infty} \frac{1}{\mu^{k-1}} < \infty$, the sequence of Lagrangian function $\{\mathcal{L}(\mathbf{X}_{k+1}, \mathbf{Z}_{k+1}, \mathbf{A}_{k+1}, \rho_{k+1})\}$ is upper bound.

3. Thirdly, we prove that the sequences of $\{\mathbf{X}_k\}$ and $\{\mathbf{Z}_k\}$ are upper bounded. Since $\|\mathbf{W}(\mathbf{Y} - \mathbf{X})\|_F^2 + \|\mathbf{Z}\|_{w,*} = \mathcal{L}(\mathbf{X}_k, \mathbf{Z}_k, \mathbf{A}_{k-1}, \rho_{k-1}) - \langle \mathbf{A}_k, \mathbf{X}_k - \mathbf{Z}_k \rangle - \frac{\rho_k}{2} \|\mathbf{X}_k - \mathbf{Z}_k\|_F^2 = \mathcal{L}(\mathbf{X}_k, \mathbf{Z}_k, \mathbf{A}_{k-1}, \rho_{k-1}) + \frac{1}{2\rho_k} (\|\mathbf{A}_{k-1}\|_F^2 - \|\mathbf{A}_k\|_F^2)$. Thus $\{\mathbf{W}(\mathbf{Y} - \mathbf{X}_k)\}$ and $\{\mathbf{Z}_k\}$ are upper bounded, and hence the sequence $\{\mathbf{X}_k\}$ is bounded by the Cauchy-Schwarz inequality

108 and triangle inequality. We can obtain that $\lim_{k \rightarrow \infty} \|\mathbf{X}_{k+1} - \mathbf{Z}_{k+1}\|_F = \lim_{k \rightarrow \infty} \rho_k^{-1} \|\mathbf{A}_{k+1} - \mathbf{A}_k\|_F = 0$ and the equation
 109 (a) is proved.

110 4. Then we can prove that $\lim_{k \rightarrow \infty} \|\mathbf{X}_{k+1} - \mathbf{X}_k\|_F = \lim_{k \rightarrow \infty} \|(\mathbf{W}^\top \mathbf{W} + \frac{\rho_k}{2} \mathbf{I})^{-1} (\mathbf{W}^\top \mathbf{W} \mathbf{Y} - \mathbf{W}^\top \mathbf{W} \mathbf{Z}_k - \frac{1}{2} \mathbf{A}_k) -$
 111 $\rho_k^{-1} (\mathbf{A}_k - \mathbf{A}_{k-1})\|_F \leq \lim_{k \rightarrow \infty} \|(\mathbf{W}^\top \mathbf{W} + \frac{\rho_k}{2} \mathbf{I})^{-1} (\mathbf{W}^\top \mathbf{W} \mathbf{Y} - \mathbf{W}^\top \mathbf{W} \mathbf{Z}_k - \frac{1}{2} \mathbf{A}_k)\|_F + \rho_k^{-1} \|\mathbf{A}_k - \mathbf{A}_{k-1}\|_F = 0$ and
 112 hence (b) is proved.

113 5. Finally, (c) can be proved by checking that $\lim_{k \rightarrow \infty} \|\mathbf{Z}_{k+1} - \mathbf{Z}_k\|_F = \lim_{k \rightarrow \infty} \|\mathbf{X}_k + \rho_k^{-1} \mathbf{A}_{k-1} - \mathbf{Z}_k + \mathbf{X}_{k+1} - \mathbf{X}_k +$
 114 $\rho_k^{-1} \mathbf{A}_{k-1} + \rho_k^{-1} \mathbf{A}_k - \rho_k^{-1} \mathbf{A}_{k+1}\|_F \leq \lim_{k \rightarrow \infty} \|\Sigma_{k-1} - \mathcal{S}_{w/\rho_{k-1}}(\Sigma_{k-1})\|_F + \|\mathbf{X}_{k+1} - \mathbf{X}_k\|_F + \rho_k^{-1} \|\mathbf{A}_{k-1} + \mathbf{A}_{k+1} -$
 115 $\mathbf{A}_k\|_F = 0$, where $\mathbf{U}_{k-1} \Sigma_{k-1} \mathbf{V}_{k-1}^\top$ is the SVD of the matrix $\mathbf{X}_k + \rho_{k-1} \mathbf{A}_{k-1}$. \square

119 2. More denoising results on the 24 high quality images from the Kodak PhotoCD dataset

120 In the main paper, we have given the PSNR results of the competing methods on the 24 high quality images from the
 121 Kodak PhotoCD dataset when the standard deviations of the additive white Gaussian noise (AWGN) are $\sigma_r = 40, \sigma_g =$
 122 $20, \sigma_b = 30$ for R, G, B channels, respectively. Here we provide more denoising results on this dataset. In Tables 1-2, we
 123 give more PSNR results on these images when the noise standard deviations are $\sigma_r = 5, \sigma_g = 30, \sigma_b = 15$ in Table 1 and
 124 $\sigma_r = 30, \sigma_g = 10, \sigma_b = 50$ in Table 2, respectively. In Figures 1-9, we give the visual comparisons of the denoised images
 125 by different methods.

126 Table 1. PSNR(dB) results of different denoising methods on 24 natural images.

Image#	$\sigma_r = 5, \sigma_g = 30, \sigma_b = 15$								
	CBM3D	MLP	TNRD	NI	NC	WNNM-1	WNNM-2	WNNM-3	MC-WNNM
1	27.25	28.06	28.62	25.00	29.55	28.16	27.95	28.15	30.20
2	29.70	31.30	32.70	27.80	29.69	32.54	31.60	31.73	34.04
3	30.34	31.98	34.07	28.02	31.93	33.91	33.68	33.52	35.55
4	29.47	31.10	32.56	27.70	32.56	32.68	31.85	31.90	34.06
5	27.31	28.59	29.35	26.14	30.00	28.83	29.00	28.91	30.05
6	28.20	29.10	29.90	26.15	28.81	29.55	29.46	29.62	31.64
7	29.73	31.60	33.46	27.22	31.63	33.09	33.29	32.86	34.24
8	27.47	28.16	28.91	25.34	30.16	29.15	29.24	29.03	29.91
9	30.07	31.63	33.55	27.86	31.54	33.19	33.20	32.95	34.53
10	29.96	31.37	33.20	27.74	33.44	32.98	33.02	32.74	34.38
11	28.73	29.85	30.87	26.98	30.16	30.45	30.14	30.21	32.10
12	30.20	31.50	33.31	27.97	31.69	33.22	32.71	32.65	34.64
13	26.18	26.69	26.98	25.14	27.97	26.49	26.42	26.62	28.30
14	27.86	29.07	29.87	26.67	29.21	29.36	29.14	29.30	31.18
15	29.91	31.58	33.13	28.04	31.17	33.22	32.34	32.36	34.27
16	29.29	30.35	31.54	27.46	32.18	31.34	31.05	31.21	33.72
17	29.50	31.09	32.52	27.81	32.80	32.09	32.00	31.85	33.61
18	27.72	28.74	29.36	26.57	28.63	28.88	28.76	28.89	30.56
19	28.98	30.18	31.35	27.25	29.79	31.34	30.77	30.95	33.10
20	30.63	31.78	33.27	27.89	29.52	33.00	32.55	32.58	34.18
21	28.50	29.58	30.54	26.86	30.99	30.02	30.03	30.03	31.69
22	28.61	29.78	30.82	27.19	30.50	30.47	29.82	30.10	32.08
23	30.60	32.66	35.06	28.17	32.82	34.72	34.37	33.94	35.16
24	27.97	28.81	29.61	26.01	30.75	29.47	29.35	29.39	30.93
Average	28.92	30.19	31.44	27.04	30.73	31.17	30.91	30.89	32.67

216

217

218

219

220

221

222

223

224

225

226

227

228

229

230

231

232

233

234

235

236

237

238

239

240

241

242

243

244

245

246

247

248

249

250

251

252

253

254

255

256

257

258

259

260

261

262

263

264

265

266

267

268

269

270

271

272

273

274

275

276

277

278

279

280

281

282

283

284

285

286

287

288

289

290

291

292

293

294

295

296

297

298

299

300

301

302

303

304

305

306

307

308

309

310

311

312

313

314

315

316

317

318

319

320

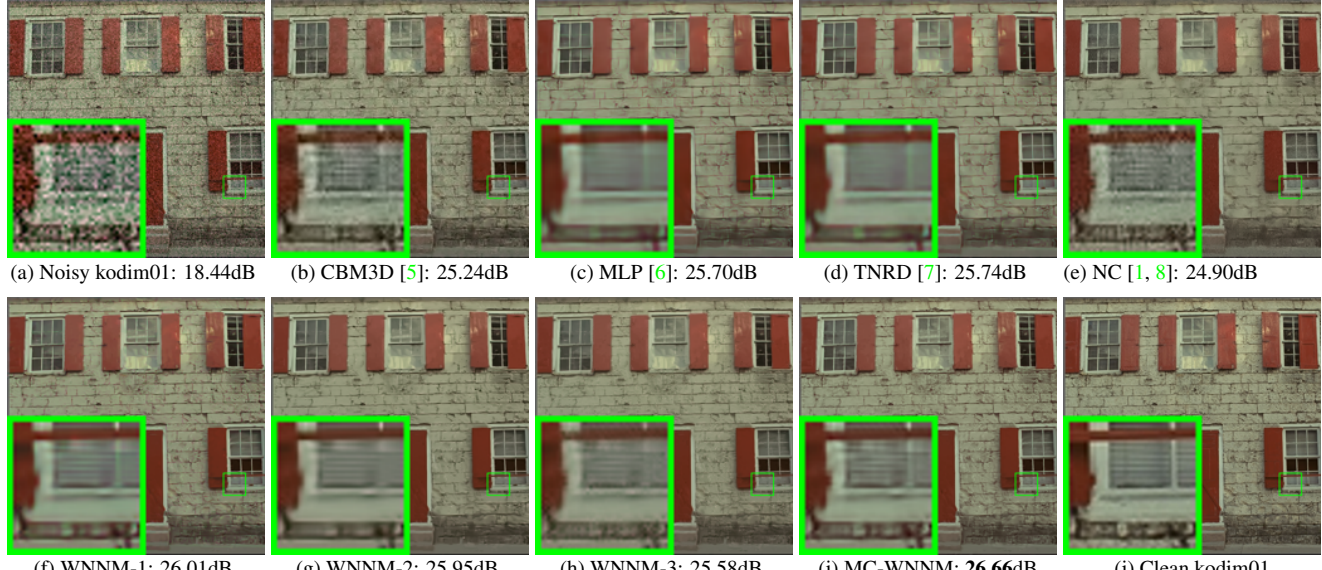
321

322

323

Table 2. PSNR(dB) results of different denoising methods on 24 natural images.

Image#	$\sigma_r = 30, \sigma_g = 10, \sigma_b = 50$								
	CBM3D	MLP	TNRD	NI	NC	WNNM-1	WNNM-2	WNNM-3	MC-WNNM
1	23.38	26.49	26.50	24.82	23.59	26.40	25.60	24.76	27.81
2	25.19	30.94	30.90	26.82	27.79	30.89	29.75	29.21	30.96
3	25.39	32.03	32.09	27.52	27.41	32.20	31.17	30.39	32.89
4	24.96	30.55	30.47	27.34	27.00	30.74	29.71	29.10	31.19
5	23.29	26.65	26.73	25.72	26.67	26.74	25.98	24.68	27.60
6	24.09	27.76	27.70	26.10	26.12	27.85	26.96	26.01	29.15
7	24.89	30.70	30.72	27.17	28.07	30.91	29.94	28.87	31.37
8	23.30	26.12	26.27	25.59	26.11	26.87	26.33	24.74	27.44
9	25.20	31.35	31.31	27.74	28.33	31.30	30.45	29.44	32.08
10	25.13	31.01	31.05	27.60	28.53	31.12	30.17	29.21	31.83
11	24.54	28.79	28.82	26.72	24.40	28.73	27.79	26.94	29.60
12	25.43	31.60	31.60	27.82	29.01	31.59	30.62	29.91	32.11
13	22.50	24.71	24.73	24.96	23.36	24.70	23.85	22.86	25.96
14	23.91	27.69	27.72	26.26	23.08	27.62	26.81	25.91	28.57
15	25.45	31.09	31.05	27.36	28.49	31.29	30.21	29.46	31.39
16	24.89	29.79	29.73	27.35	27.10	29.84	28.85	28.13	31.10
17	25.12	30.26	30.24	27.15	27.54	30.11	29.35	28.43	31.08
18	23.83	27.26	27.26	26.05	26.15	27.32	26.18	25.28	28.32
19	24.63	29.40	29.39	27.06	27.41	29.78	28.87	28.05	30.53
20	26.43	31.16	31.27	26.43	26.92	31.25	30.43	29.41	31.55
21	24.24	28.26	28.27	26.66	27.18	28.22	27.45	26.40	29.29
22	24.51	29.03	29.06	26.83	27.64	29.02	27.81	27.18	29.57
23	25.55	32.87	32.75	27.60	23.75	32.58	31.46	30.50	32.34
24	23.85	27.06	27.13	25.86	27.05	27.50	26.63	25.55	28.32
Average		24.57	29.27	29.28	26.69	26.61	29.36	28.43	27.52
									30.09

Figure 1. Denoised images of different methods on the image "kodim01" degraded by AWGN with different standard deviations of $\sigma_r = 40, \sigma_g = 20, \sigma_b = 30$ on R, G, B channels, respectively. The images are better to be zoomed in on screen.

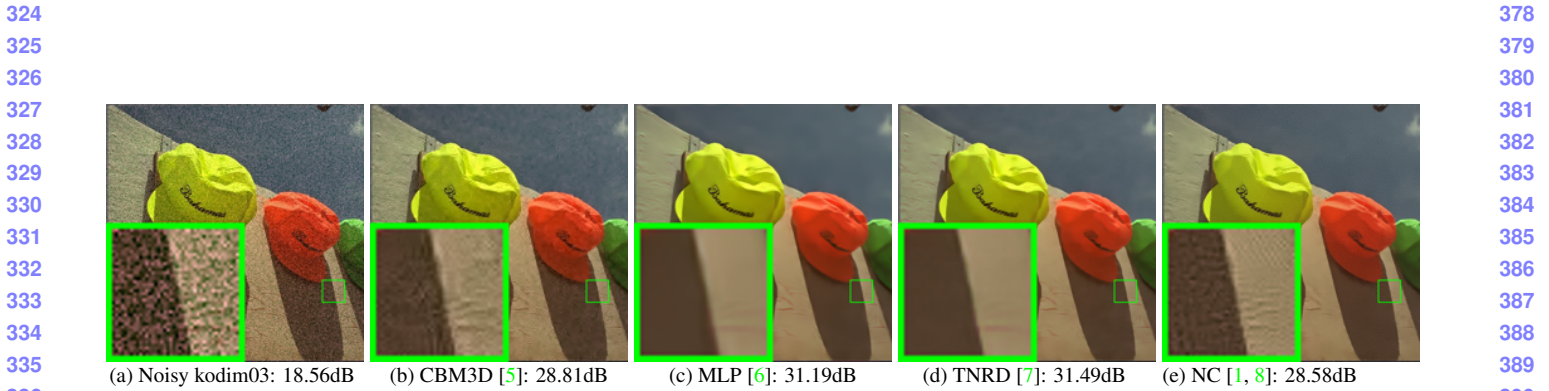


Figure 2. Denoised images of different methods on the image “kodim03” degraded by AWGN with different standard deviations of $\sigma_r = 40$, $\sigma_g = 20$, $\sigma_b = 30$ on R, G, B channels, respectively. The images are better to be zoomed in on screen.

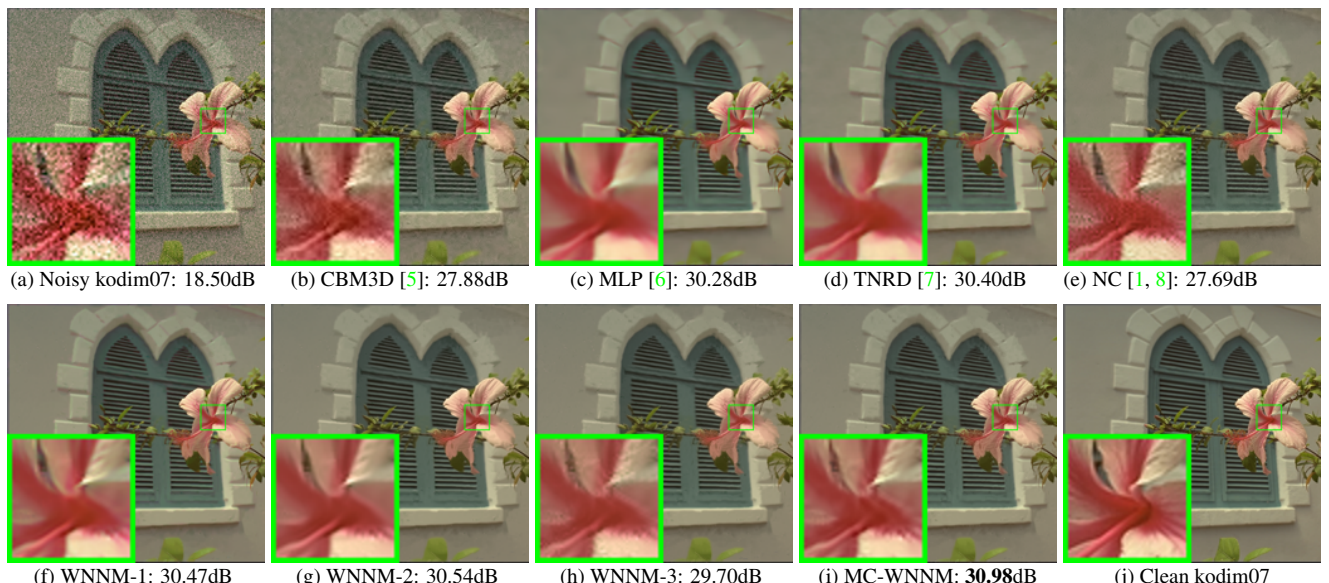


Figure 3. Denoised images of different methods on the image “kodim07” degraded by AWGN with different standard deviations of $\sigma_r = 40$, $\sigma_g = 20$, $\sigma_b = 30$ on R, G, B channels, respectively. The images are better to be zoomed in on screen.

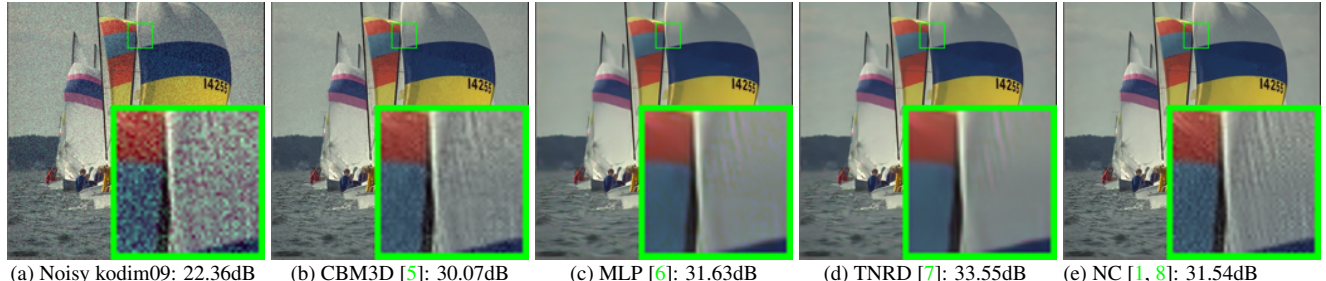
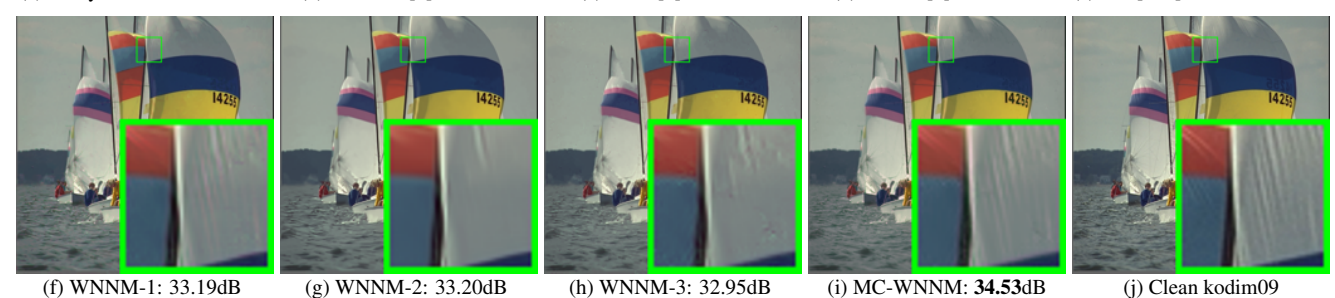
432
433
434486
487
488444
445
446
447
448
449
450
451
452498
499
500
501
502
503
504
505
506453
454
455507
508
509

Figure 4. Denoised images of different methods on the image “kodim09” degraded by AWGN with different standard deviations of $\sigma_r = 5, \sigma_g = 30, \sigma_b = 15$ on R, G, B channels, respectively. The images are better to be zoomed in on screen.

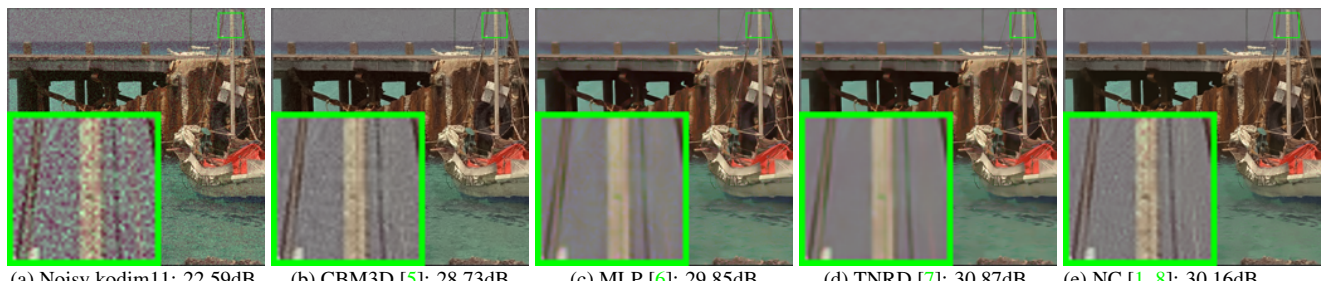
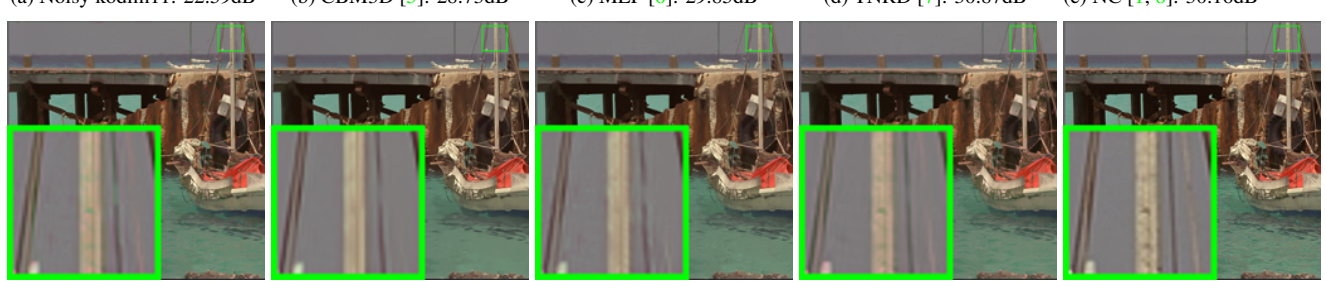
456
457
458
459
460
461510
511
512
513
514
515
516
517
518
519
520
521
522
523471
472
473
474
475
476
477
478
479524
525
526
527
528
529
530
531
532480
481
482534
535
536

Figure 5. Denoised images of different methods on the image “kodim11” degraded by AWGN with different standard deviations of $\sigma_r = 5, \sigma_g = 30, \sigma_b = 15$ on R, G, B channels, respectively. The images are better to be zoomed in on screen.

483

537

484

538

485

539

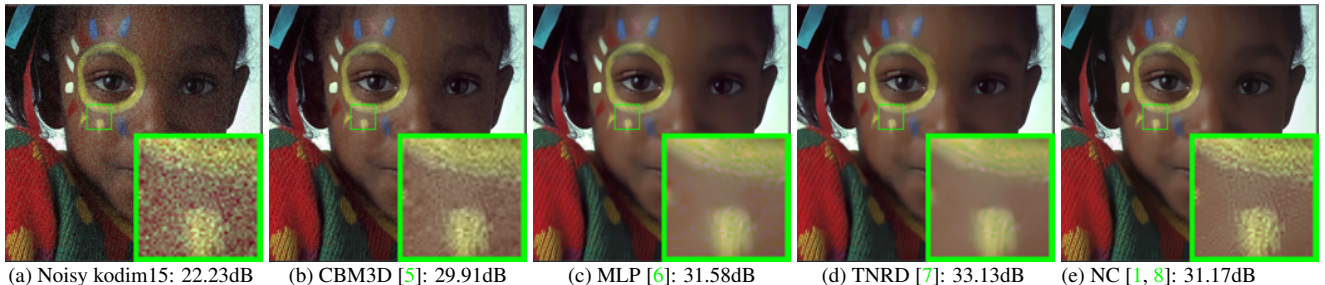


Figure 6. Denoised images of different methods on the image “kodim15” degraded by AWGN with different standard deviations of $\sigma_r = 5, \sigma_g = 30, \sigma_b = 15$ on R, G, B channels, respectively. The images are better to be zoomed in on screen.

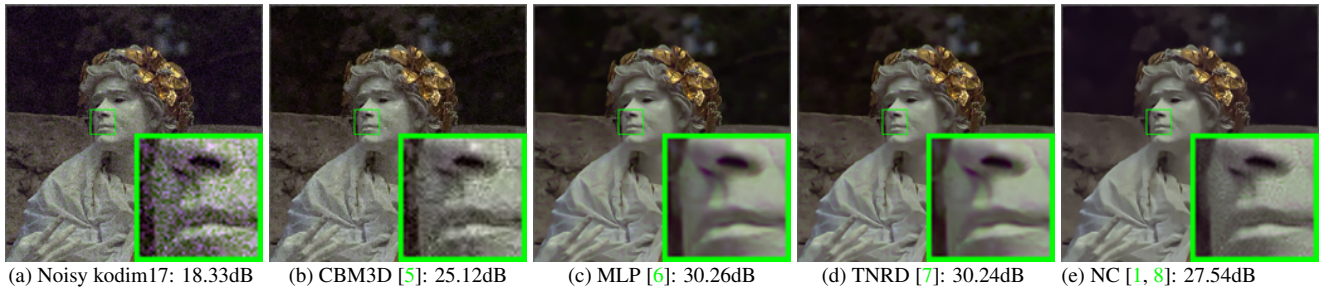


Figure 7. Denoised images of different methods on the image “kodim17” degraded by AWGN with different standard deviations of $\sigma_r = 30, \sigma_g = 10, \sigma_b = 50$ on R, G, B channels, respectively. The images are better to be zoomed in on screen.

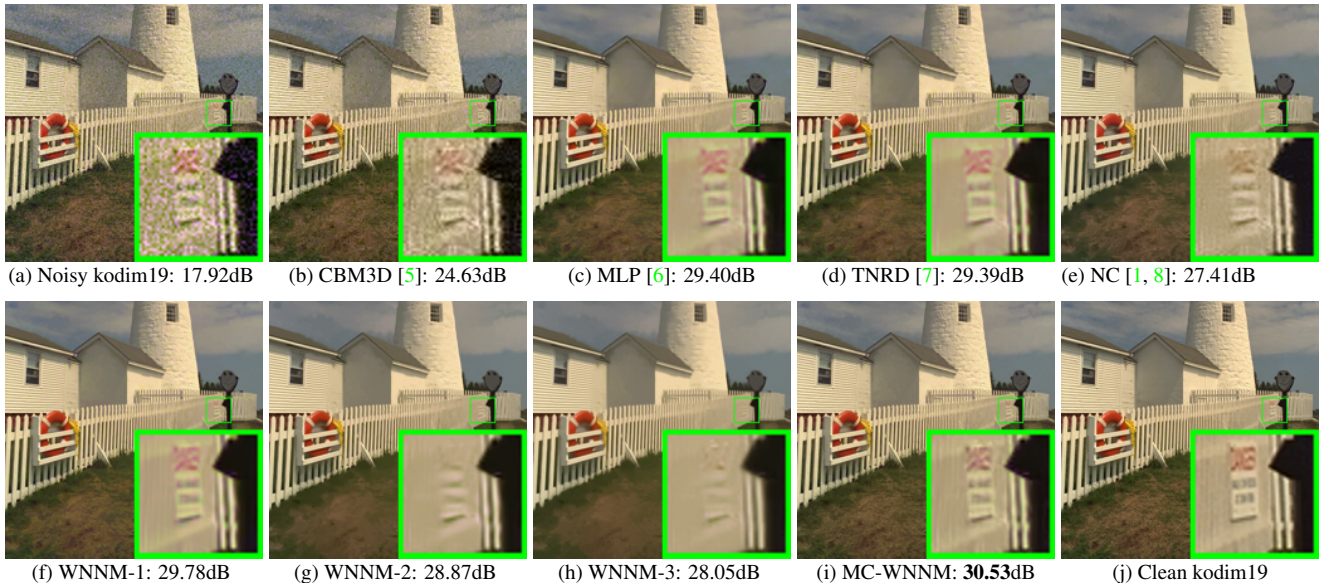


Figure 8. Denoised images of different methods on the image “kodim19” degraded by AWGN with different standard deviations of $\sigma_r = 30$, $\sigma_g = 10$, $\sigma_b = 50$ on R, G, B channels, respectively. The images are better to be zoomed in on screen.

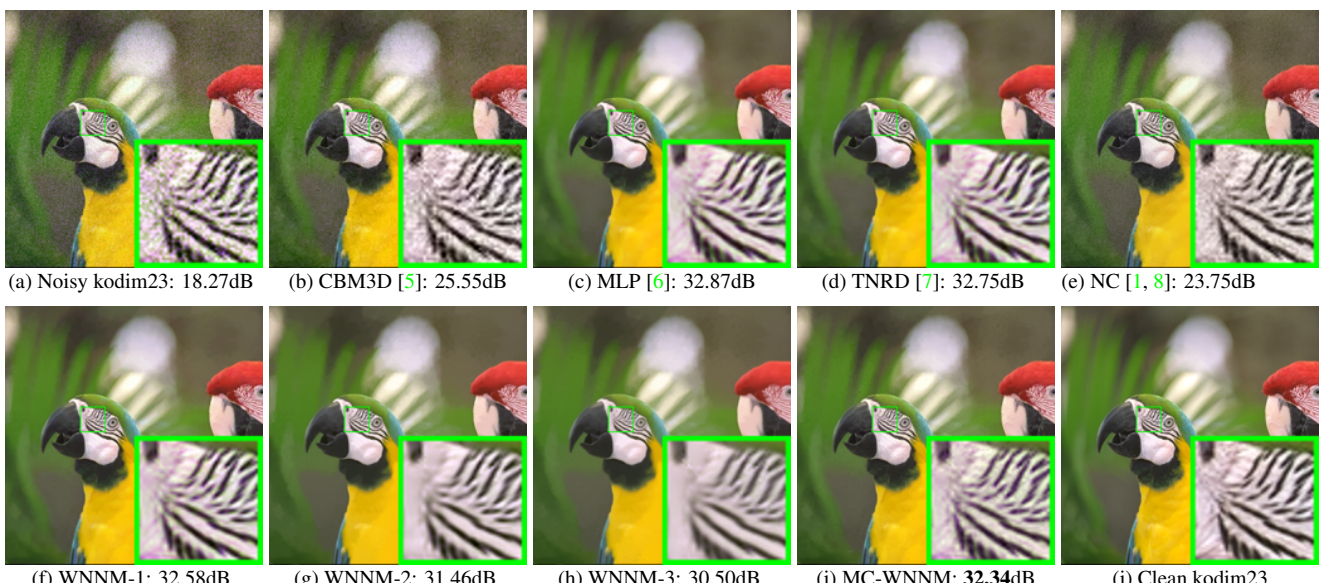


Figure 9. Denoised images of different methods on the image “kodim23” degraded by AWGN with different standard deviations of $\sigma_r = 30$, $\sigma_g = 10$, $\sigma_b = 50$ on R, G, B channels, respectively. The images are better to be zoomed in on screen.

3. More visual comparisons of denoised images by different methods on the real noisy images of the dataset [1]

In this section, we give more comparisons of the state-of-the-art denoising methods on the dataset [1]. The real noisy images in dataset [1] have no “ground truth” images and hence we only compare the visual quality of the denoised images by different methods. As can be seen from Figures 10-12, the proposed MC-WNNM method performs better than the competing methods.

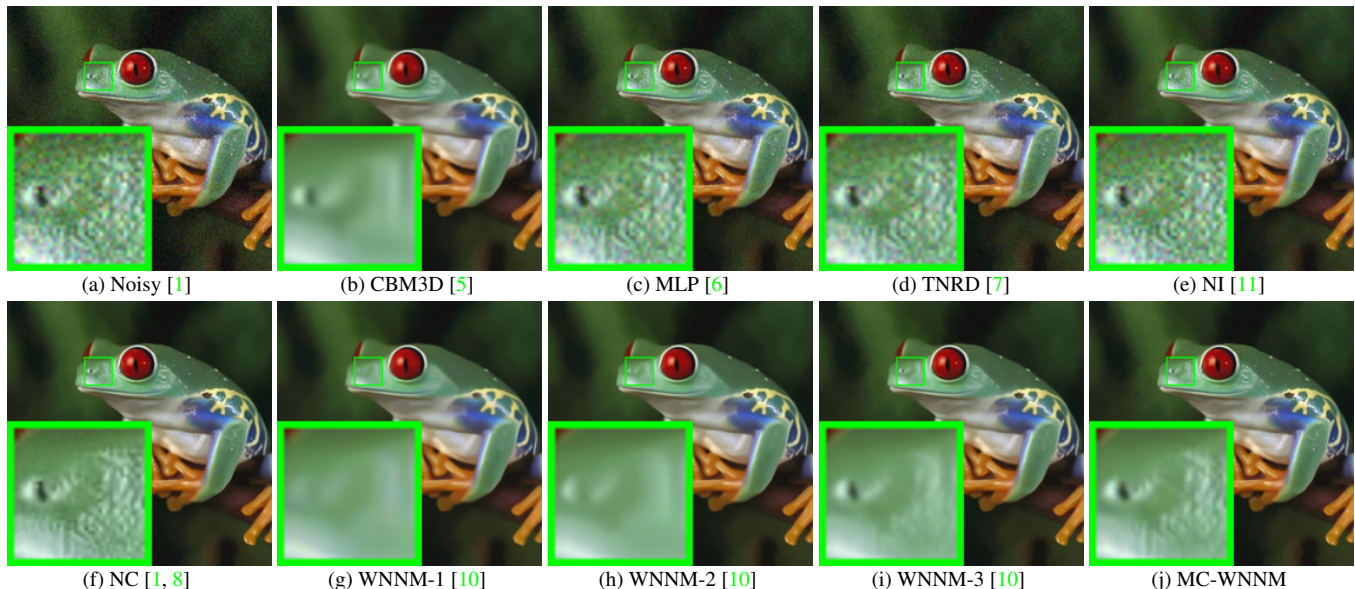


Figure 10. Denoised images of the real noisy image “Frog” [1] by different methods. The images are better to be zoomed in on screen.

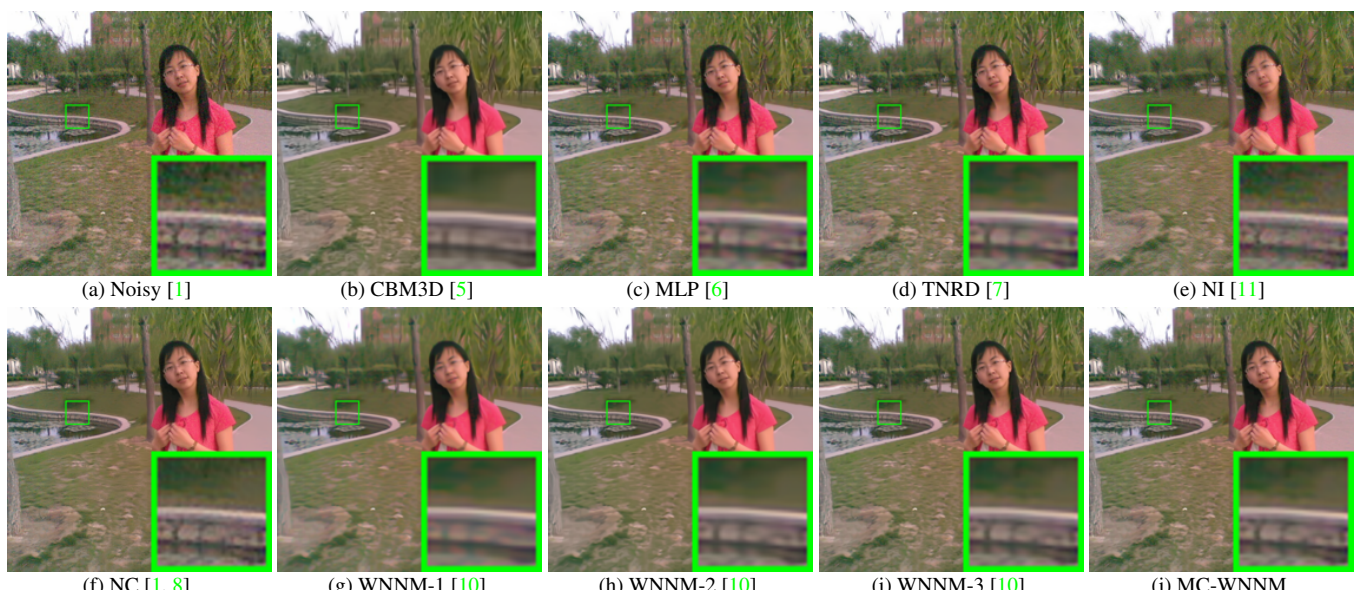


Figure 11. Denoised images of the real noisy image “Gril” [1] by different methods. The images are better to be zoomed in on screen.

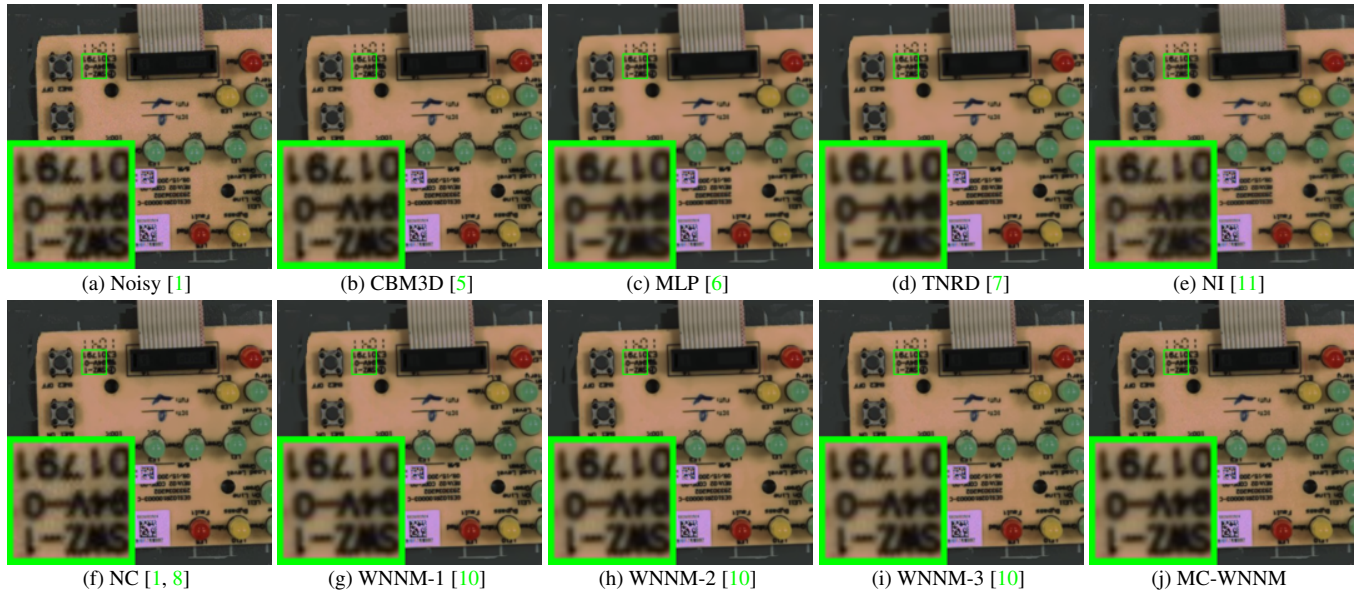


Figure 12. Denoised images of the real noisy image “Circuit” [1] by different methods. The images are better to be zoomed in on screen.

4. More visual comparisons of denoised images by different methods on the real noisy images of the dataset [2]

In this section, we provide more comparisons of the proposed method with the state-of-the-art denoising methods on the 15 cropped real noisy images used in [2]. In this dataset, each scene was shot 500 times under the same camera and camera setting. The mean image of the 500 shots is roughly taken as the “ground truth”, with which the PSNR can be computed. As can be seen from Figures 13-16, in most cases, our proposed method achieves better performance than the competing methods. This validates the effectiveness of the proposed MC-WNNM method for real noisy image denoising.

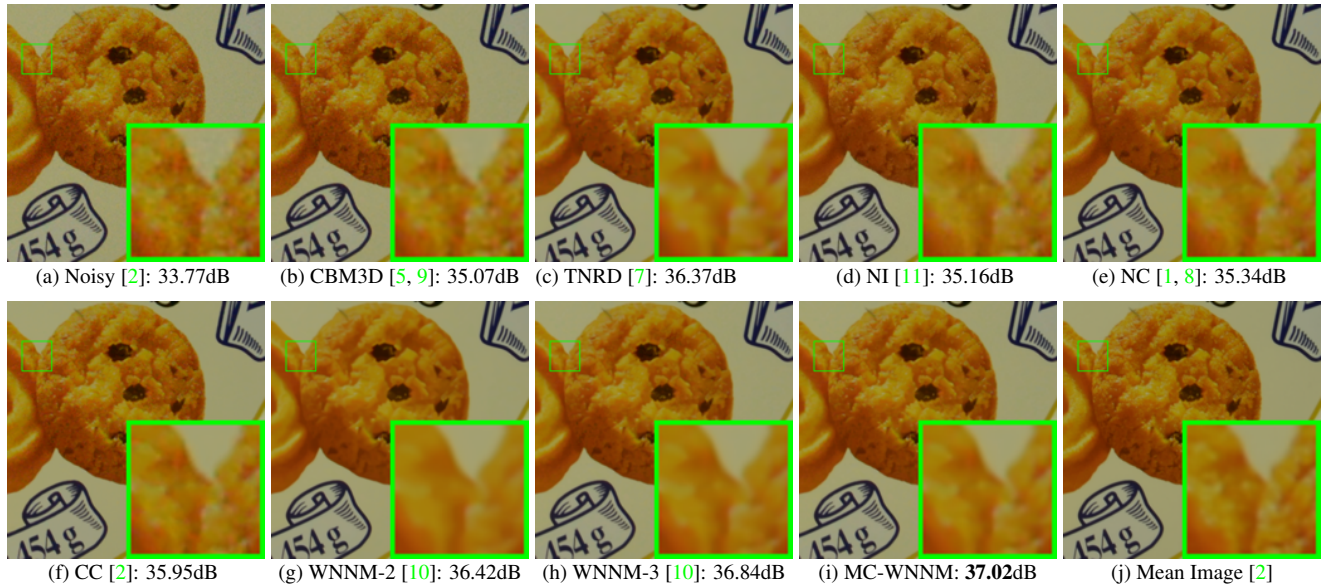


Figure 13. Denoised images of a region cropped from the real noisy image “Nikon D600 ISO 3200 2” [2] by different methods. The images are better to be zoomed in on screen.

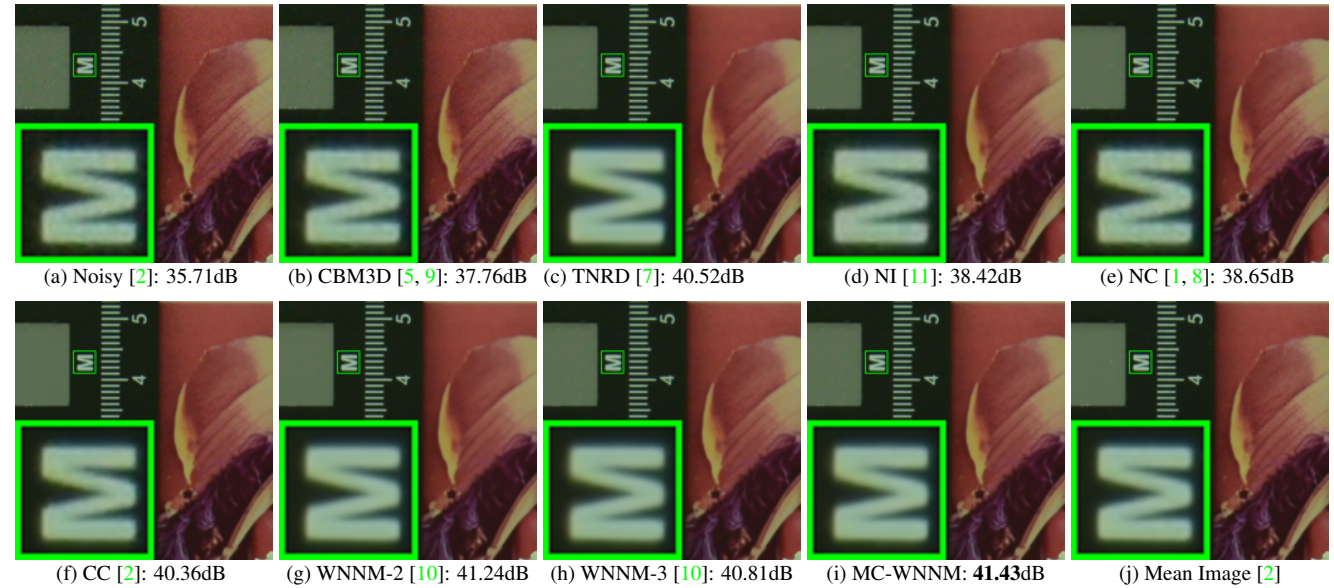


Figure 14. Denoised images of a region cropped from the real noisy image “Nikon D800 ISO 1600 2” [2] by different methods. The images are better to be zoomed in on screen.

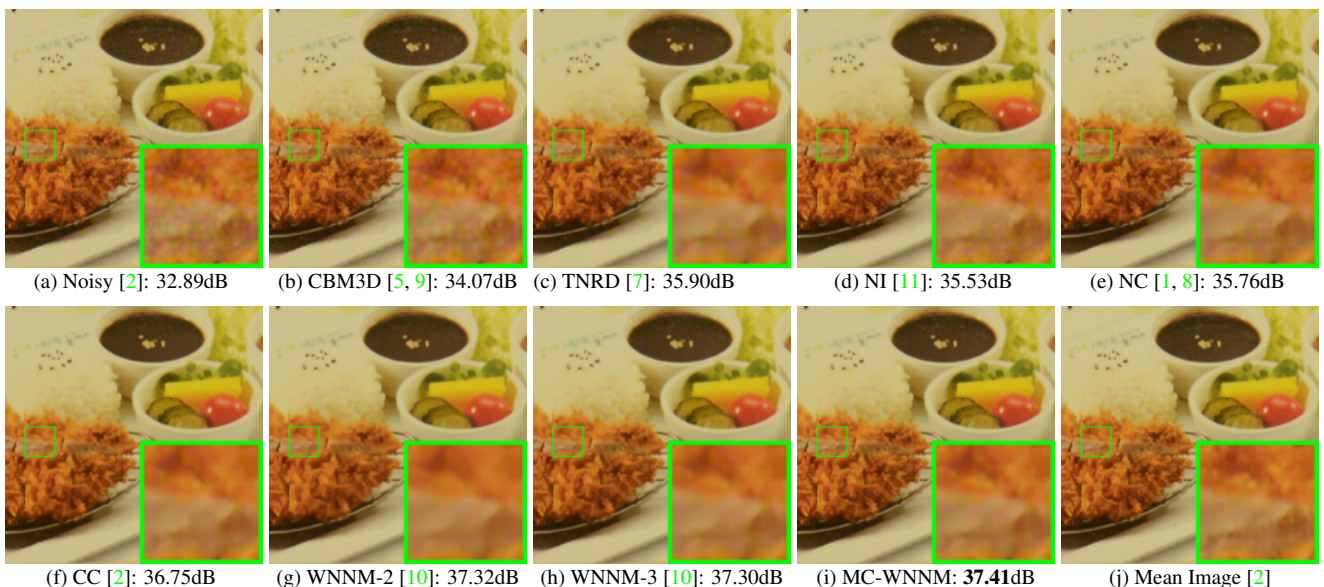


Figure 15. Denoised images of a region cropped from the real noisy image “Nikon D800 ISO 3200 2” [2] by different methods. The images are better to be zoomed in on screen.

References

- [1] M. Lebrun, M. Colom, and J. M. Morel. The noise clinic: a blind image denoising algorithm. <http://www.ipol.im/pub/art/2015/125/>. Accessed 01 28, 2015. 1, 3, 4, 5, 6, 7, 8, 9, 10, 11
- [2] S. Nam, Y. Hwang, Y. Matsushita, and S. J. Kim. A holistic approach to cross-channel image noise modeling and its application to image denoising. *IEEE Conference on Computer Vision and Pattern Recognition (CVPR)*, pages 1683–1691, 2016. 1, 9, 10, 11
- [3] C. Eckart and G. Young. The approximation of one matrix by another of lower rank. *Psychometrika*, 1(3):211–218, 1936. 1
- [4] S. Gu, Q. Xie, D. Meng, W. Zuo, X. Feng, and L. Zhang. Weighted nuclear norm minimization and its applications to low level vision. *International Journal of Computer Vision*, pages 1–26, 2016. 1

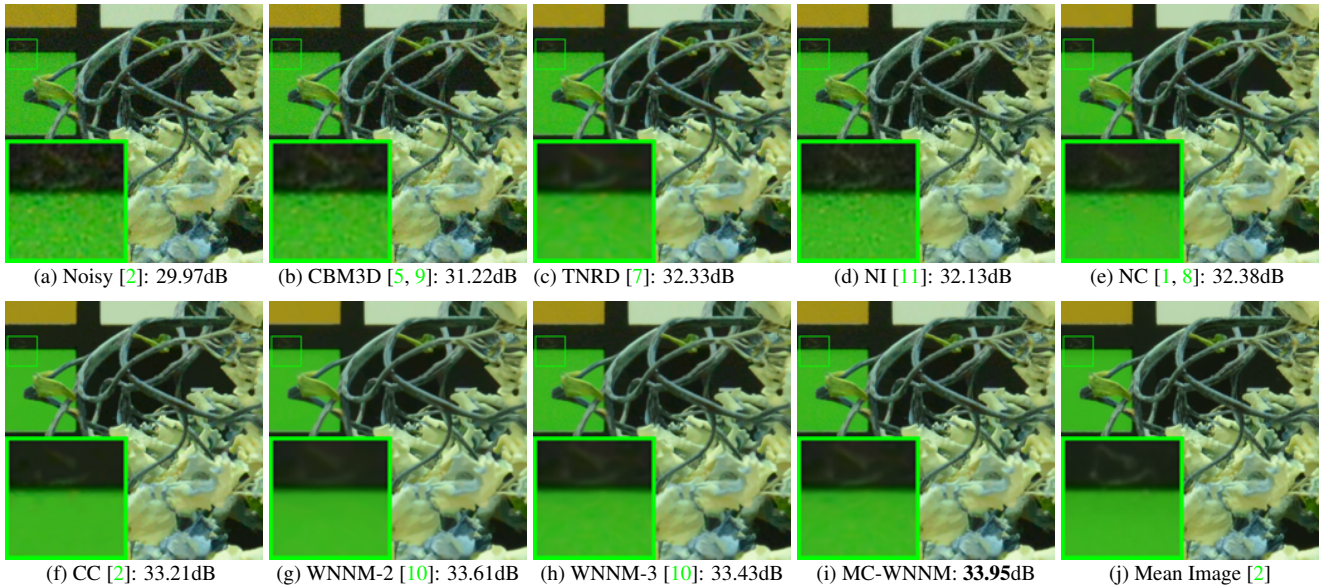


Figure 16. Denoised images of a region cropped from the real noisy image “Nikon D800 ISO 6400 2” [2] by different methods. The images are better to be zoomed in on screen.

- [5] K. Dabov, A. Foi, V. Katkovnik, and K. Egiazarian. Color image denoising via sparse 3D collaborative filtering with grouping constraint in luminance-chrominance space. *IEEE International Conference on Image Processing (ICIP)*, pages 313–316, 2007. 3, 4, 5, 6, 7, 8, 9, 10, 11
- [6] H. C. Burger, C. J. Schuler, and S. Harmeling. Image denoising: Can plain neural networks compete with BM3D? *IEEE Conference on Computer Vision and Pattern Recognition (CVPR)*, pages 2392–2399, 2012. 3, 4, 5, 6, 7, 8, 9
- [7] Y. Chen, W. Yu, and T. Pock. On learning optimized reaction diffusion processes for effective image restoration. *IEEE Conference on Computer Vision and Pattern Recognition (CVPR)*, pages 5261–5269, 2015. 3, 4, 5, 6, 7, 8, 9, 10, 11
- [8] M. Lebrun, M. Colom, and J.-M. Morel. Multiscale image blind denoising. *IEEE Transactions on Image Processing*, 24(10):3149–3161, 2015. 3, 4, 5, 6, 7, 8, 9, 10, 11
- [9] K. Dabov, A. Foi, V. Katkovnik, and K. Egiazarian. Image denoising by sparse 3-D transform-domain collaborative filtering. *IEEE Transactions on Image Processing*, 16(8):2080–2095, 2007. 9, 10, 11
- [10] S. Gu, L. Zhang, W. Zuo, and X. Feng. Weighted nuclear norm minimization with application to image denoising. *IEEE Conference on Computer Vision and Pattern Recognition (CVPR)*, pages 2862–2869, 2014. 8, 9, 10, 11
- [11] Neatlab ABSoft. Neat Image. <https://ni.neatvideo.com/home>. 8, 9, 10, 11